Soft Matter

PAPER

View Article Online
View Journal | View Issue

Cite this: *Soft Matter*, 2026, **22**, 2499

The effect of charge density on the viscoelasticity and underwater adhesion of entangled complex coacervates from semi-rigid polysaccharides

Maxime Precheur,[a] Ali Kanan,[a] Alexei Dmitrievitsj Filippov,[a] Kylian Virieux,[b] Stéphane Trombotto,[b] Fouzia Boulmedais[a] and Mehdi Vahdati*[a]

Received 10th December 2025,
Accepted 17th February 2026

DOI: 10.1039/d5sm01220a

rsc.li/soft-matter-journal

We analyzed the effect of charge density (CD) on the phase behavior, viscoelasticity, and underwater adhesion of complex coacervates formed from high-molecular-weight, semi-flexible, bio-sourced polyelectrolytes. For this, hyaluronic acid (HA) was complexed with chitosan (CHI) of different degrees of deacetylation (DD) at pH 5.0. It was found that increasing CHI deacetylation enhanced macroion pairing, expanding the two-phase region of the phase diagram. Time–salt superposition (TSS) was successfully applied, allowing us to rescale the linear viscoelastic response of all the HA–CHI series onto individual master curves, indicating that the relaxation dynamics of all series are controlled by macroion pairing. The TSS curves were further collapsed onto a universal master curve *via* a so-called time–salt–charge density superposition (TSCDS). This first report of TSCDS for entangled complex coacervates revealed that the salt sensitivity of the dynamics depends on the charge density, which is in contrast with reports on flexible polyelectrolytes. It is proposed that this difference is due to the interplay between the persistence length of the semi-flexible polyelectrolytes and kinetic trapping in these entangled systems. The underwater adhesion strength (σ_{max}) of HA–CHI reached 74 kPa at 0.2 M NaCl. Replacing CHI's acetyl moiety with a less polar butyryl group (*but*-CHI) at a given DD had a slight effect on the composition and viscoelastic properties. However, HA–*but*-CHI had the highest underwater adhesion near physiological salinity (σ_{max} of 110 kPa and an adhesion energy of 18 J m^{-2}), placing it among the most high-performing coacervate-based underwater adhesives without an external trigger.

1. Introduction

Polyelectrolyte complex coacervates are a class of soft materials obtained *via* the associative phase separation of oppositely charged polyelectrolytes in water, resulting in a dilute phase called the supernatant and a polymer-rich phase called a complex coacervate. This phase separation is driven by the release of counterions and the reorganization of water molecules, resulting in the formation of the so-called macroion pairs between the oppositely charged repeat units of the two PE.[1–6] Macroion pairs act as transient crosslinks, whose number density and strength can be controlled by the salt concentration, among other parameters. Due to their widely tuneable mechanical properties and high-water contents, complex coacervates have been proposed for diverse applications such as tissue engineering, drug delivery, embolic agents, and biomedical sealants and adhesives.[7–10]

Unlike the well-known effects of salt concentration, which have been extensively studied in systems of various polymer chemistries and molecular weights (MWs),[3,11–21] understanding the influence of the polymer charge density (CD) is a more recent endeavor with a series of systematic studies based on flexible polyelectrolytes. Recently, the group of Laaser[22] used polymers synthesized from mixtures of charged and neutral comonomers to systematically vary the fraction of charged *versus* neutral repeat units, thereby examining CD effects on the phase behavior and viscoelasticity of model complex coacervates. Systems at CD above 60 mol% were shown to be in the charge-dominated regime. In this regime, the relative hydrophilicity/hydrophobicity of the neutral comonomer had no tangible effect, and the phase behavior and rheology were dominated by electrostatics. Similarly, Neitzel and coworkers showed that decreasing the CD using hydrophilic comonomers resulted in more swollen coacervates and smaller binodal boundaries.[23] Kamperman's group further explored how variations in CD with either randomly distributed hydrophilic[24] or hydrophobic[25] comonomers affect

[a] *University of Strasbourg, CNRS, Institut Charles Sadron, UPR22, 67200 Strasbourg, France. E-mail: mehdi.vahdati@ics-cnrs.unistra.fr*
[b] *Ingénierie des Matériaux Polymères, UMR 5223, Université Claude Bernard Lyon 1, CNRS, INSA Lyon, Université Jean Monnet Saint-Etienne, F-69622 Villeurbanne, France*

the viscoelastic and adhesion properties of complex coacervates. They reported distinct and opposing behaviors in the charge-dominated and hydrophobicity-dominated regimes, pointing out that observing hydrophobic effects necessitated sufficiently hydrophobic groups capable of forming local associations.[24,25] Finally, Perry and collaborators decoupled the effects of CD and hydrophobicity in the phase composition and viscoelasticity of model complex coacervates.[26] They achieved this by varying the CD of random copolymers containing either hydrophilic or hydrophobic neutral comonomers and by adjusting the ratio between hydrophilic and hydrophobic comonomers at a fixed CD. Overall, these reports highlighted the importance of comonomer chemistry and the distinctions between charge-dominated and hydrophobicity-dominated regimes, where the dynamics become respectively slower and faster at higher charge densities.

However, all of these studies have focused on low-molecular-weight synthetic polyelectrolytes, leaving a knowledge gap regarding the role of CD in complex coacervates based on high-molecular-weight polyelectrolytes. Another aspect that has received little attention is the role of the persistence length, l_p, of the polymers involved in complex coacervation. In fact, the charge density and the persistence length of charged macromolecules are not decoupled. The presence of charges along the chain is known to increase the chain stiffness by an electrostatic contribution to the persistence length, $l_{p,e}$. For a given polyelectrolyte, $l_{p,e}$ is a function of many parameters, including the comonomer composition, the salt concentration, the level of hydration, and the CD. The overall persistence length of a polyelectrolyte is the sum of these two contributions, $l_p = l_{p,0} + l_{p,e}$.[27] Compared to most synthetic polyelectrolytes, which are inherently flexible, polysaccharides are semi-flexible polymers with persistence lengths that are 10 to 100 times larger,[28,29] and the extent of stiffening depends on the type of polysaccharide and the experimental conditions.

Hyaluronic acid (HA) and chitosan (CHI) are among the most widely studied bio-sourced polyelectrolytes due to their large availability, low toxicity, and suitability to a variety of biomedical applications.[30–33] HA is a linear alternating copolymer of N-acetyl glucosamine and glucuronic acid ($pK_a \sim 2.5$), known for its strong hydration and inherent chain rigidity ($l_p \sim$ 5–15 nm).[34,35] CHI ($l_p \sim$ 4–8 nm) is a linear polymer typically obtained from the partial deacetylation of chitin, resulting in a copolymer of neutral *N*-acetyl glucosamine and ionizable glucosamine ($pK_a \sim 6.5$).[29,36,37] Depending on the degree of deacetylation (DD), MW, and pH, CHI shows different levels of solubility in water.

Complex coacervates based on HA and CHI have been the subject of several recent investigations. Kamperman's group, who reported on the phase behavior and rheological properties of low-MW (30–50 kg mol^{-1}) HA–CHI complex coacervates, elucidated the role of various interactions at pH 4.0 and 6.0. It was shown that at pH 6.0, in the vicinity of CHI's pK_a, HA–CHI form dynamically-arrested domains *via* hydrogen bonding and hydrophobic interactions, resulting in salt-insensitive complexes.[38] However, at pH 4.0, the complex coacervates had the typical behavior of unentangled viscoelastic liquids with salt-sensitive dynamics. Perry's group[39] studied the viscoelasticity of medium-MW (50–200 kg mol^{-1}) HA–CHI complex coacervates, which appeared as entangled viscoelastic liquids, although the authors did not comment on the presence of entanglements. As expected, adding salt at pH 4.5 (where both polymers are charged) resulted in increased swelling, faster chain dynamics, and lower plateau moduli. Balima and coworkers[40] reported stretchable hydrogels based on high-MW CHI (600 kg mol^{-1}) and low-MW HA (70 kg mol^{-1}) around physiological pH. The hydrogels were formed based on entanglements among CHI chains as well as macroion pairing, hydrogen bonding, and hydrophobic interactions.

Our group studied the relationships between the viscoelastic and underwater adhesive properties of high-MW (400–500 kg mol^{-1}) HA–CHI complex coacervates at pH 5.0, where both polymers are almost fully charged.[30] These complex coacervates were characterized as entangled viscoelastic liquids, with the onset of the rubbery plateau appearing at low salt concentrations. While these materials were sufficiently soft to meet the Dahlquist criterion for adhesion (plateau modulus below 0.1 MPa at 1 Hz), they were not highly dissipative. Nevertheless, they had adhesion strengths as high as 40 kPa when immersed in their own supernatant.[41] Recently, Parisi's group[42] reported on the viscoelastic and adhesive properties of HA–CHI complex coacervates of symmetric and asymmetric combinations of low, medium, and high molecular weights at pH 4.0. While the low-MW system appeared unentangled, the medium- and high-MW systems appeared as entangled physical gels at low salt concentrations. In particular, they highlighted the critical role of the relatively stiffer and hydrated HA in enhancing the salt resistance and decreasing the salt-sensitivity of the plateau modulus. The authors reported wet adhesion strengths of 20 to 160 kPa and adhesion energies of 1 to 10 J m^{-2} depending on the MW combination. While different reports have used CHI of different DD, the effect of this parameter on its complex coacervation with HA has not been investigated. This kind of study would provide insights into the effects of CD for the complex coacervation of high-MW, semi-flexible polyelectrolytes.

In this study, we aim to examine HMW, stoichiometric HA–CHI complex coacervates based on three CHI of different degrees of deacetylation, namely 71, 88, and 98 mol% (Fig. 1; we note that CHI's degree of deacetylation (DD) is equivalent to its linear charge density (CD), but the abbreviations should not be confused). We also explore a chemically modified CHI, where the acetyl moiety of the neutral comonomer is replaced with a less polar butyryl moiety. To minimize any effects from the polymer M_W, all chitosan polymers used have comparable weight-average M_W ($\sim$600 kg mol^{-1}) and dispersity ($Đ$ = 1.5–1.8) and the same HA ($M_W \sim$ 1000 kg mol^{-1}, $Đ$ = 1.9) was used in the whole study (Table 1). Compositional analysis of the dense and dilute phases to determine the total polymer, water, and salt content was performed *via* thermogravimetric analysis. Linear rheology and underwater pull-off experiments were used to study their viscoelasticity and underwater adhesive properties of the complex coacervates.

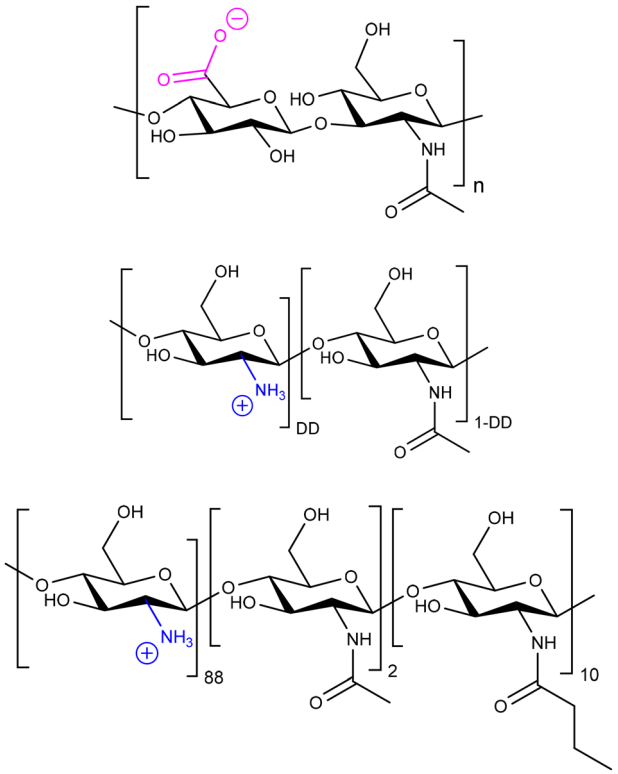

Fig. 1 Structures of the polymers used in this study (from top to bottom): hyaluronic acid (HA), chitosan of different degrees of deacetylation (CHI-DD), and butyryl chitosan with a DD of 88% (*but*-CHI-88).

Table 1 Macromolecular characteristics of the hyaluronic acid (HA), chitosans of different degrees of deacetylation (CHI-DD), and butyryl chitosan with a DD of 88% (*but*-CHI-88) used in this study; DP_w: weight-average degree of polymerization, DD: deacetylation degree, and DS: degree of substitution

Polymer	M_w (kg mol^{-1})	$Đ$	DP_w	DD (%)	DS (%)
HA	1016	1.9	5384	50	0
CHI-71	646	1.8	3768	71	0
CHI-88	580	1.5	3509	88	0
but-CHI-88	576	1.6	3433	88	10
CHI-98	625	1.8	3862	98	0

2. Materials and methods

2.1. Materials

Two high molecular weight chitosan (CHI, base form), with a deacetylation degree (DD) of 88% and 98% (confirmed *via* ^{1}H NMR), were purchased from Glentham and Mahtani Chitosan, respectively, and referred to as CHI-88 and CHI-98, respectively (Fig. 1). Their weight average molecular weight, measured *via* size exclusion chromatography (SEC), was 580 kg mol^{-1} ($Đ$ = 1.50) for CHI-88 and 625 kg mol^{-1} ($Đ$ = 1.75) for CHI-98. High molecular weight hyaluronic acid (HA) was purchased from Biosynth with a weight-average molecular weight, measured by SEC, of 1016 kg mol^{-1} ($Đ$ = 1.90). The characterization performed on the polymers is detailed in the SI. Butyric anhydride and other reagents and solvents for the synthesis were provided by Sigma-Aldrich. Sodium chloride (NaCl) with 99.5% purity was purchased from Fisher Chemical. Milli-Q® water was used in all experiments. pH adjustments were made using small quantities of concentrated solutions of HCl or NaOH.

2.2. Synthesis

In this study, a re-acetylated chitosan with a DD of 71% and a chitosan modified with butyric anhydride, with a DD of 88% and a degree of substitution (DS) of 10%, are referred to as CHI-71 and *but*-CHI-88, respectively (Fig. 1). CHI-71 and *but*-CHI-88 were prepared according to the N-acetylation method previously described by Garreau *et al.*[43] Briefly, 1 g of CHI-98 was dissolved in a 200 mL water/1,2-propanediol mixture (50 : 50 v/v) with acetic acid in a stoichiometric amount of glucosamine units. Acetic anhydride for CHI-71 (200 mg) or butyric anhydride for *but*-CHI-88 (85 mg) diluted in 1,2-propanediol (10 mL) was added dropwise at $T < 10$ °C, and the reaction medium was vigorously stirred for 12 h at RT, then filtered through 3 µm to 0.8 µm mixed cellulose ester (MCE) membranes (Millipore, France). CHI-71 and *but*-CHI-88 were precipitated by the addition of aqueous ammonia (28% w/w) to reach pH 8–9, washed repeatedly with deionized water until neutral pH, and freeze-dried with a mass yield of 86% and 82%, respectively. The weight average molecular weight, determined by SEC, were 646 kg mol^{-1} ($Đ$ = 1.80) for CHI-71 and 576 kg mol^{-1} ($Đ$ = 1.59) for *but*-CHI-88.

2.3. Preparation of HA–CHI complex coacervates

Stock solutions of the individual polymers and NaCl were prepared gravimetrically based on dry mass. CHI-71 was dissolved at 1 wt% in 0.03 M HCl by extensive stirring for 72 h at 50 °C. CHI-88 was dissolved at 2 wt% in 0.09 M HCl by extensive stirring for 24 h at room temperature. CHI-98 was dissolved at 1 wt% in 0.04 M HCl by extensive stirring for 24 h at room temperature. *But*-CHI was dissolved at 1 wt% in 0.05 M HCl by extensive stirring for 72 h at room temperature. The pH was adjusted to 5 using 1.0 M HCl and 1.0 M NaOH. HA was dissolved at 2.5 wt% in Milli-Q® water, and the pH was adjusted to 5 using a concentrated solution of HCl. Finally, a 5 M stock solution of NaCl at pH 5.0 was made.

All complex coacervates were prepared at charge stoichiometry at pH 5.0, a condition at which both HA and CHI are nearly fully ionized.[38,39,44] The total concentration of the charged groups in the complex coacervates was set at 0.038 M, corresponding to a total polymer concentration of 1.2, 1.1, 1.0, and 1.0 wt% for HA–CHI-71, HA–CHI-88, HA–CHI-100, and HA–*but*-CHI-88, respectively. A Multipette® M4 (Eppendorf) pipette equipped with different tips adapted to viscous and non-viscous solutions was used to prepare the samples. The appropriate volume of the NaCl stock solution was first added to 4.37 mL of HA under continuous stirring. Subsequently, the necessary volume of each CHI solution (6.9, 2.6, 4.6, and 5.4 mL of CHI-71, CHI-88, CHI-100, or *but*-CHI-88 solution, respectively) was introduced as a single addition to form the corresponding CHI–HA mixtures. Stirring was continued for 3 h, after which the samples were transferred to Falcon® tubes and left to

equilibrate for 24 h. The samples were subsequently centrifuged at 9000 rpm for 30 min. Each preparation was performed in duplicate on different days using independent stock solutions to ensure reproducibility. Images of the four complex coacervate series at different salt concentrations are provided in Fig. S1 in the SI.

2.4 Thermogravimetric analysis (TGA)

We used thermogravimetric analysis to characterize the composition of the coacervates and supernatants. TGA experiments were performed on a TG 209 F1 Libra (Netzsch) using 85 or 300 μL alumina crucibles under an air flow of 100 mL min^{-1}. The sample, either a coacervate or a supernatant, was heated from room temperature up to 150 °C at a rate of 10 °C min^{-1}, where it was held for 20 min to remove all the water, followed by heating to 1000 °C at a rate of 20 °C min^{-1}. The weight loss of the sample (in percentage) was recorded relative to the initial weight. The water, polymer, and salt content of the complex coacervates (CC) and supernatant (SN) were determined as described in the SI.

2.5. Underwater linear rheology

Linear rheology experiments were performed on a Discovery HR-20 (TA Instruments) rheometer equipped with a Peltier plate and an immersion cell. All rheological experiments were carried out at 37 °C in the supernatant corresponding to each sample. The geometry used was a sandblasted stainless steel flat plate with a radius of 10 mm. The sample was first slowly squeezed to a gap of h_0 = 500 μm, and the axial force was allowed to relax below 1.0 N. The immersion medium was then added and allowed to equilibrate at the test temperature. A solvent trap was used to avoid evaporation from the supernatant. Frequency sweeps on all the samples were performed within the linear regime at 0.1% strain.

2.6. Underwater pull-off tests

Underwater pull-off tests were performed using the same rheometer and setup described in the underwater rheology section, following a procedure detailed in our previous study.[30] The pull-off tests immediately followed each frequency sweep test, with the same sample thickness (h_0) of 500 μm. The pull-off force (F) was measured as a function of displacement (h) as the probe was removed at a constant pull-off velocity of 100 μm s^{-1} or a nominal strain rate of 0.2 s^{-1}. The nominal stress (σ) and nominal strain (ε) were respectively calculated as:

$$\sigma = \frac{F}{A_0} \quad (1)$$

$$\varepsilon = \frac{h - h_0}{h_0} \quad (2)$$

where A_0 is the surface area of the probe. The maximum pull-off stress was taken as the underwater adhesion strength σ_{max}. The adhesion energy (W_{adh}), *i.e.*, the energy required to create a unit surface area of the adhesive, was calculated as:

$$W_{adh} = h_0 \int_0^{\varepsilon_{max}} \sigma \cdot d\varepsilon \quad (3)$$

The reported values are an average of three measurements of independently prepared and tested samples.

3. Results and discussion

3.1 Phase behavior

We first investigated the impact of the salt concentration on the composition of the complex coacervates.[15,23,24,41,45–47] All complex coacervates were prepared at pH 5.0, where the charges of HA and CHI are nearly balanced, resulting in an approximately 1 : 1 charge ratio between the polymers.[38,39,44] The effect of salt was examined over a range of NaCl concentrations from 0.0 to 0.8 M. Representative images of the four complex coacervate systems are shown in Fig. S1 (SI). TGA measurements were carried out to determine the composition of the complex coacervates and the supernatants. Fig. 2A shows the state diagram for each HA–CHI series by plotting the molar concentration of salt *versus* polymer. In each case, an approximative binodal boundary is presented as a guide to the eye. Moreover, the salt resistance of each HA–CHI series, marked with a star, was estimated from the doping level, as described elsewhere.[3,41,48] Briefly, the doping level, y, is defined as the fraction of the macroion pairs dissociated by condensed counterions in the dense phase:

$$y = \frac{[NaCl]_{count}}{[PE]} \quad (4)$$

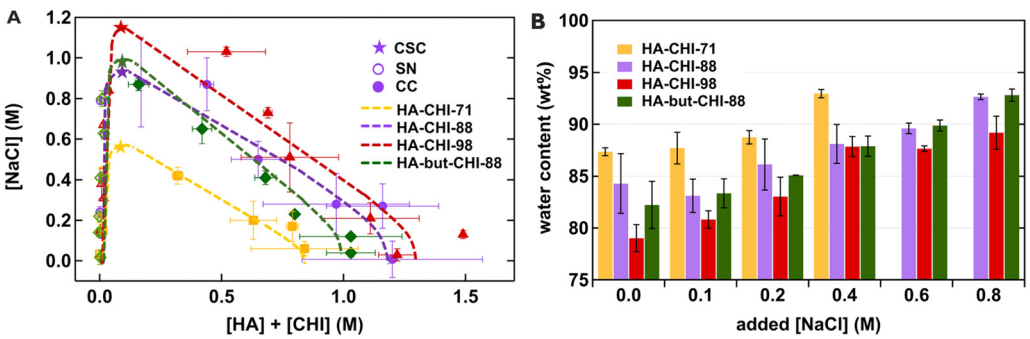

Fig. 2 Compositional analysis of different HA–CHI complex coacervate series: (A) state diagrams showing the salt concentration as a function of the polymer concentration, and (B) the water content of the polymer-rich phase as a function of the added NaCl concentration.

where [PE] is the total number of macroions, *i.e.* $[PE^+] + [PE^-]$. The ratio of the total number of small ions to the macroions is equal to or more than the doping level, given that the small ions in the dense phase may exist as free co-ions or condensed counterions.

$$r = \frac{[NaCl]_{tot}}{[PE]} = \frac{[NaCl]_{free} + [NaCl]_{count}}{[PE]} \quad (5)$$

The parameters y and r are thus correlated *via*:

$$y = \frac{r}{1+r} \quad (6)$$

From eqn (6), y can be calculated from experimentally determined values of r. Extrapolating the doping level to 1 then gives an estimation for the salt resistances of each HA–CHI series (Fig. S3 in the SI). The equivalent state diagram with the concentrations in wt% is shown in Fig. S5 in the SI. The apparent differences between the two state diagrams are due to the consideration of the changes in the density of the two phases, which modifies molar, and not mass, concentrations. In general, the binodal curves in Fig. 2A exhibit the characteristic behavior of polyelectrolyte complex coacervates.[45,47] As the salt concentration increases, the complex coacervate phase becomes more dilute in polymers until phase separation is suppressed at sufficiently high salt concentrations. All the supernatants are polymer-poor, indicating a strong phase separation and the exclusive partitioning of the polyelectrolytes into the polymer-rich phase. In the following, we investigate the effects of chitosan CD and hydrophobicity on the phase behavior and the estimated salt resistance of these complex coacervates.

As shown in Fig. 2A, the state diagram of HA–CHI complex coacervates broadens with increasing the DD of CHI, or equivalently, its CD. This trend is consistent with previous reports: increasing the CD increases the number of macroion pairs (stickers) per chain, which enhances the potential entropic gain from the release of the counterions and, hence, the overall driving force for coacervation.[23,24,26,49,50] In the case of HA–CHI-88 and HA–CHI-98 series, kinetic trapping occurs at relatively low salt concentrations resulting in non-equilibrium complexes. This is reflected in the large error bars observed below 0.2 M NaCl (Fig. 2A).[5,51–53] This effect is less visible for HA–CHI-71 series. Kinetic trapping results from the long relaxation times inherent to high charge density and low salt concentration systems (see the underwater rheology section below). These effects are amplified by the high molecular weight and large persistence length of the polymers, causing the system to fall out of equilibrium. This is in agreement with a recent report on the dynamics of HA–CHI complex coacervates of different molecular weights by Mohamed Yunus and coworkers.[42] This point will be discussed later in this article.

The salt resistance of HA–CHI-71, HA–CHI-88, and HA–CHI-98 was estimated by extrapolating the doping level to 1. The results of this extrapolation, shown in Fig. S3 in the SI, were found to be 0.78, 0.98, and 1.1 M NaCl, for HA–CHI-71, HA–CHI-88, and HA–CHI-98, respectively. Although these values are consistent with our experimental observations for CHI-88 and CHI-98, no phase separation was observed at 0.6 M NaCl for HA–CHI-71. This apparent discrepancy is likely due to the smaller number of data points used in fitting the doping level in the latter case. Nonetheless, the estimated salt resistance values are consistent with the state diagrams, indicating that increasing the CD enhances the stability of the complex coacervates against salt. At comparable DD, the salt resistances are in the same range as the values reported previously for high-molecular-weight HA–CHI and higher than those for lower molecular weight systems.[30,38,39,42] Indeed, higher molecular weights result in diminished translational entropy of coacervation, resulting in a broader two-phase region in the phase diagram.

For flexible, hydrophilic, fully charged polymers, Spruijt and co-workers showed that the equilibrium salt resistance reaches an asymptotic value already at routinely accessible molecular weights corresponding to a DP on the order of 10^2.[50] In contrast, the scaling of the critical salt concentration with persistence length and effective monomer–solvent interaction pushes the critical salt resistance asymptote to higher salt concentrations and higher DP, above 10^4. Then, the salt resistance is controlled only by the solvent quality towards the polymers in the complex, the CD and the persistence length. The effect of persistence length on salt resistance has not yet been systematically studied, and the semi-flexible chains with varying affinity to the solvent used in this work might not be at their salt resistance asymptote chain length.

We also plotted the apparent tie-lines connecting the compositions of the supernatant and the complex coacervate phases for all samples in Fig. S4 in the SI. At low salt concentrations (0.0 to 0.4 M NaCl), the tie-lines exhibit a horizontal slope, while at higher salt concentrations (0.4 to 0.8 M NaCl), a slightly positive slope is observed for the HA–CHI-88 and HA–CHI-98 systems. Positively tilted tie lines indicate an endothermic complexation, with the small ions preferring to act as co-ions rather than counter-ions.[54] This is generally the case for model systems based on flexible, synthetic polyelectrolytes. The semi-flexibility of HA and CHI and the inherently strong hydration of these polymers (especially HA) and of their complex coacervates are conducive to an endothermic complexation. That said, other effects, such as the Donnan breakdown and kinetic trapping, may also contribute to the change in the slope of the tie lines.

As proposed by Schlenoff, the ion content of polyelectrolyte complex coacervates, and thus the slope of the tie lines, is determined by the modification of an ideal Donnan equilibrium by possible enthalpic contributions from the complexation of the fixed macroions.[54,55] In an ideal mixture with no enthalpic contribution to the complexation free energy, the Donnan potential generated by the fixed charges excludes mobile counterions from the polymer-rich phase at low ionic strengths. In this regime, most salt ions act as counterions and compete with macroion pairing. At higher salt concentrations, this selectivity vanishes, allowing mobile ions to diffuse into the coacervate, corresponding to an increased presence of free co-ions within the coacervate, a phenomenon known as

Donnan breakdown.[41,55] An analogous change in the tie-line slope has been reported by Ramírez Marrero *et al.*,[26] where an increase in salt concentration resulted in a shift from negative or nearly horizontal to positive for high CD systems. In our case, this change in the slope of the tie lines is not tangible for the HA–CHI-71 system, likely due to its lower salt resistance, which makes it difficult to observe the Donnan breakdown. We note that this argument is general and not specific to positively tilted tie lines, and other parameters such as the enthalpy of complexation and kinetic trapping may also contribute to the tie line slope.[54]

The water content of the complex coacervates as a function of the added NaCl concentration is presented in Fig. 1B. All the complex coacervates are water-rich materials with 78 to 93 wt% water depending on the DD and [NaCl]. Increasing the salt concentration increases the water content in all systems, with a few exceptions due to kinetic trapping. Among the different HA–CHI series, a higher CD (or DD) results in a lower water content across all initial salt concentrations, in good agreement with the state diagrams. This trend also suggests that CHI's neutral comonomer (acetyl glucosamine) is relatively hydrophilic. Moreover, we find that the HA–CHI-71 presented here has a similar water content to a previously reported system based on a comparable CHI (in terms of DD and molecular weight) and a relatively smaller HA (400 kg mol^{-1} in the previous work *vs.* 1016 kg mol^{-1} here).[30] This indicates that at very large DP, HA's molecular weight has a small influence on the water content.[13,41] In other words, the strong hydration of HA is probably insensitive to the DP for very large degrees of polymerization. Overall, these highlight the critical role of the CD in the composition of these bio-sourced complex coacervates.

Comparing the HA–*but*-CHI-88 and HA–CHI-88 series, with CHI of the same CD, no significant differences in their state diagram, salt resistance, and water content are seen within the experimental error of our measurements. This suggests that the composition of the complex coacervate is relatively insensitive to moderate changes in the hydrocarbon content of the non-ionic (neutral) comonomer of CHI. As reported by Huang *et al.*[22] and Ramírez Marrero *et al.*,[26] a threshold amount of aliphatic characteristic must be present before hydrophobic effects begin to modify the phase behavior. In the present case, the CD is sufficiently high for the phase behavior to be dominated by electrostatic interactions, which could explain why the chemical modification of CHI-88 to *but*-CHI-88 does not alter the composition of their complex coacervates with HA. Literature comparison reveals that the butyryl modification is too sparse (10% of all the repeat units) and the acyl group too short (C_4) to influence the composition in any significant way, as shown by Huang and Laaser,[22] the composition of hydrophobically modified complex coacervates at a given CD only varies with the side chain length above a critical *n*-alkyl group size at a neutral comonomer fraction of 10%. For modification with butyl side-chains, they obtained no difference in the salt resistance, whereas modification with hexyl moieties led to an increase. We conclude that the glucosamine comonomer of CHI is sufficiently hydrophilic, at the comonomer fractions and acyl chain length used in this work, to have no tangible influence on the state diagrams of complexation with HA.

Overall, CHI's CD exerts a significant influence on the phase behavior of these bio-sourced complex coacervates and can therefore be used as a control parameter to adjust their composition, salt resistance, and salt partitioning behavior. In contrast, moderate variations in CHI's side chain length (from acetyl to butyryl) at a fixed CD have no substantial effect on the composition. Building on this understanding, we next examine how these factors influence the mechanical properties of these HA–CHI complex coacervates.

3.2 Viscoelasticity of the HA–CHI complex and time–salt superposition

Underwater rheology measurements were performed at 37 °C with each sample immersed in its own supernatant. We first investigated the HA–CHI-88 system, which will serve as the reference throughout this study. Fig. 3A and B show the storage and loss moduli, and the corresponding loss factor, from frequency sweeps on HA–CHI-88 complex coacervates prepared at different NaCl concentrations. The samples from 0.0 to 0.6 M NaCl are characterized as soft, entangled gels in the rubbery plateau, where the viscoelastic behavior is dominated by the storage modulus (G'). At 0.6 M NaCl, the dynamic moduli are close to a crossover at the low end of the frequency window studied. The sample at 0.8 M NaCl clearly displays a crossover

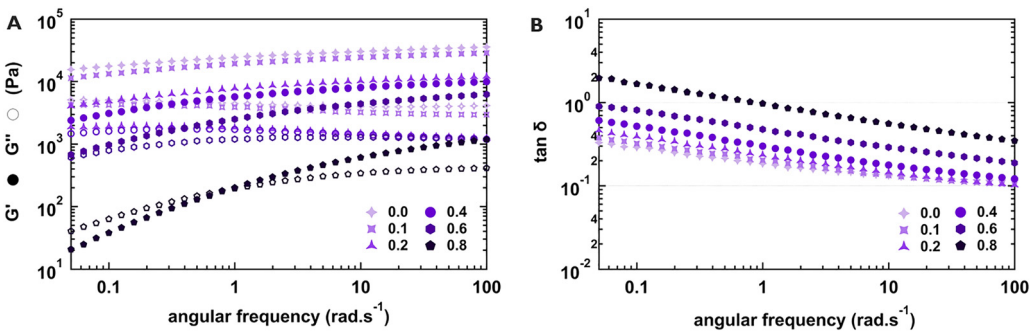

Fig. 3 Linear viscoelastic properties of the HA–CHI-88 complex coacervates prepared at 37 °C: (A) storage modulus (G') and loss modulus (G''), and (B) loss factor, $\tan\delta = G''/G'$ as a function of angular frequency.

of the storage and loss (G'') moduli, corresponding to the sticky reptation time, τ_{rep}. Increasing the salt concentration results in softer and more dynamic complex coacervates, as evidenced by the shift in the crossover to higher frequencies at 0.8 M compared to 0.6 M NaCl.

We similarly performed underwater rheology measurements on the other HA–CHI series. The frequency sweeps of HA–CHI-71, HA–CHI-98, and HA–*but*-CHI-88 at different salt concentrations are provided in Fig. S7 in the SI. The behavior of the samples from each series is generically similar to those of HA–CHI-88. They all behave as soft viscoelastic solids within the lower frequency end of the rubbery plateau, with lower dynamic moduli and shorter relaxation times as the salt concentration increases. This solid-like behavior at low salt concentration for each system is also in line with our visual observation of the samples (images presented in Fig. S1 in the SI). The only exception to this general behavior is the HA–CHI-98 sample at 0.8 M NaCl that appears as a soft critical gel, characterized by much lower dynamic moduli and a frequency-independent loss tangent around 0.4. The viscoelastic behavior of this sample is probably governed by a combination of electrostatic and other weak interactions at this high salt concentration (in the proximity of the binodal boundary) and is thus essentially different from all the other samples. For these reasons, we did not include this sample in the following analyses.

Next, we studied the feasibility of time–salt superposition (TSS) within each series. TSS, which has been reported in many complex coacervate systems,[15,30,39,41,56,57] is applicable when the relaxation times of all the modes have the same dependence on the salt concentration, making the dynamics at different salt concentrations self-similar.[2,58] When this is the case, all the frequency sweep data can be rescaled onto a master curve using a single salt-dependent shift factor. We assessed the self-similarity of the dynamics across the studied salt concentrations within each series *via* $\tan\delta$ curves, van Gurp-Palmen plots, and Cole–Cole plots (see Fig. S7–S9 in the SI). These analyses confirmed that the relaxation dynamics of all the samples within each series have the same dependence on the salt concentration, suggesting that the macroion pairs are the main type of stickers at work.[2,59]

TSS was thus performed for each series using the respective 0.4 M NaCl sample as the reference. The master curves of the different series are presented in Fig. 4A–D. The horizontal and vertical shift factors a_s and b_s, applied to obtain these master curves, are presented in Fig. 5A and B, respectively. All the master curves reveal the lower frequency end of a broad rubbery plateau at 0.4 M NaCl. In the case of HA–CHI-88, the crossover of G' and G'' give a relatively long sticky reptation time ($\tau_{rep} = 1/\omega_c$) of 210 s and a crossover plateau (G_c) of 0.8 kPa (Fig. 4B). The crossover is not observed in the HA–CHI-98 and HA–CHI-71 master curves. In the former case, this is due to a lack of self-similarity in dynamics due to the appearance of other weak interactions at 0.8 M NaCl (see Fig. S7 in the SI). In the latter case, the sample at 0.6 M NaCl is a single-phase solution above the salt resistance, with an expectedly different dynamic response.

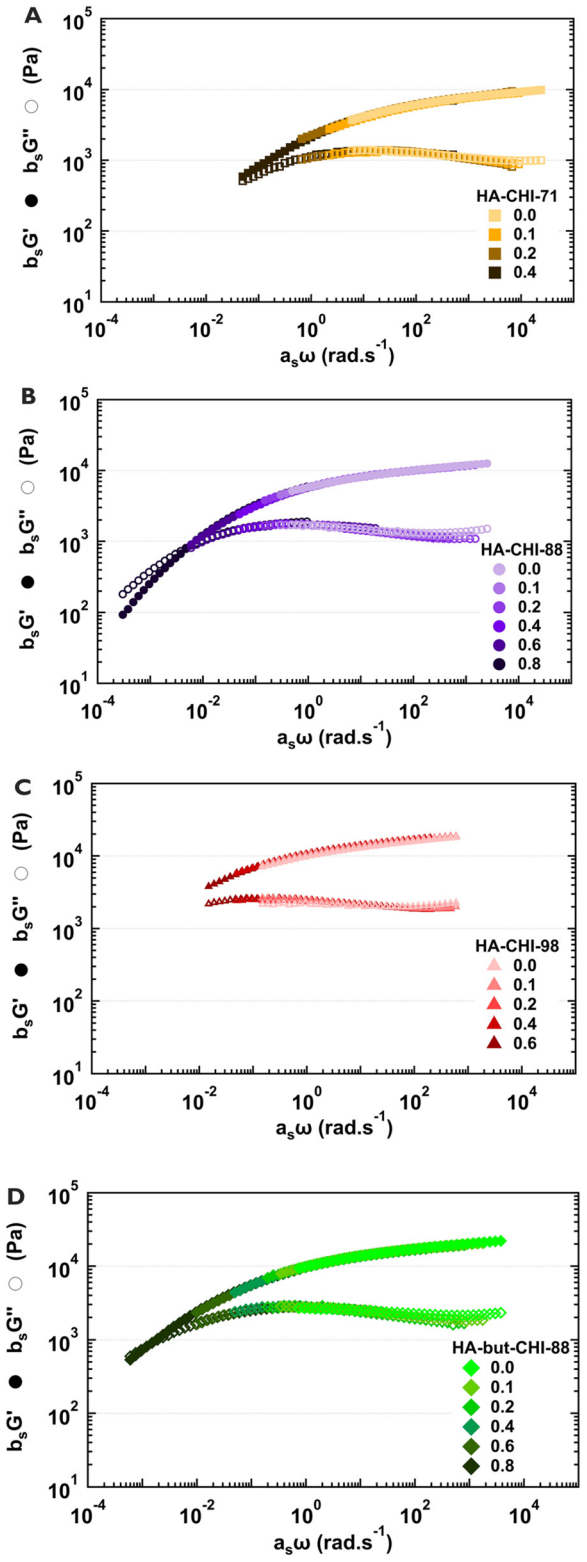

Fig. 4 Rescaled dynamic moduli of (A) HA–CHI-71, (B) HA–CHI-88, (C) HA–CHI-98, and (D) HA–*but*-CHI-88 complex coacervates using time–salt superposition (TSS), taking the 0.4 M NaCl sample of each series as the reference.

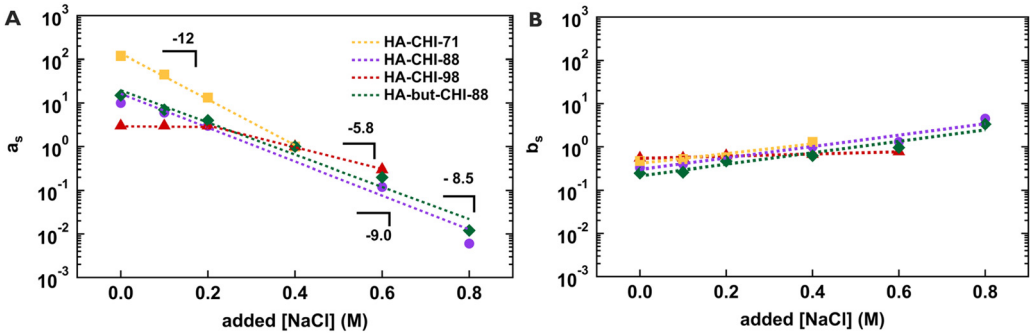

Fig. 5 Time-salt superposition (A) horizontal a_s and (B) vertical b_s shift factors as a function of the added salt concentration.

Before comparing the TSS master curves, it is worth noting that the TSS extension of the viscoelastic window in the case of our HA–CHI complex coacervates is much larger than those in previous studies on these polysaccharides. Most previous systems have highly dynamic and unentangled viscoelastic liquids in the terminal regime.[30,38,44] One successful TSS attempt with high molecular weight HA (200 kg mol^{-1}) and CHI (50–190 kg mol^{-1}) at pH 4.5 revealed the terminal region and the transition to the lower frequency window of the rubbery plateau. In contrast to our successful application of TSS, Mohamed Yunus and coworkers reported the failure of TSS for entangled HA–CHI at pH 4.0, which they ascribed to the presence of salt-insensitive modes such as reptation and hydration-mediated processes.[42] However, the authors did not attempt to apply a vertical shift factor, as we have done here. Moreover, Kamperman's group[38] and Kayitmazer's group,[44] who reported soft critical gels obtained from HA and CHI, found that the dynamics were influenced not only by electrostatic interactions but also by relatively long-lived interactions such as hydrogen bonding and hydrophobic interactions. This was due to the higher preparation pH around 6 or higher, which is near the pK_a of chitosan.[60–62] This made TSS in the rubbery plateau impossible, as the dynamics were controlled by different types of stickers with different salt concentration dependencies. In contrast to these studies, the feasibility of TSS for our HA–CHI samples at pH 5.0 suggests that macroion pairs are the dominant salt-dependent stickers controlling the relaxation dynamics at pH 5.0. Other relaxation processes, such as reptation, do not seem to alter the salt-dependence of the macroion pairs to the point that they disturb TSS. The success of TSS shows that other weak interactions, such as hydrophobic interactions and hydrogen bonding, have no influence on the viscoelasticity of these materials under the experimental conditions of this study (pH 5.0), since such interactions are differently affected by [NaCl].

For a more straightforward comparison of the TSS master curves of the different HA–CHI series, they are gathered in Fig. S11 in the SI. The plateau modulus of HA–CHI-71, HA–CHI-88, and HA–CHI-98 at a high frequency, *e.g.*, at 10 rad s^{-1}, is 5, 8, and 10 kPa, respectively. The increase is proportional to the polymer content of the complex coacervates (0.32, 0.65, and 0.78 M on a monomer basis for HA–CHI-71, HA–CHI-88, and HA–CHI-98, respectively), which indicates that the contribution of the macroion type stickers to the shear modulus is negligible compared to that of the entanglements. In other words, the network's elasticity at short time scales is dominated by the entanglement strands rather than the strands between the ion pairs. A large contribution of entanglements reflects the high molecular weight and the large polymer concentration (5–15 wt% at 0.4 M NaCl) in the complex coacervates. Regarding the dynamics at a given salt concentration, the relaxation times are expected to be longer with a larger number of stickers per chain at higher charge densities. While this is indeed the case, the deceleration of the dynamics at 0.4 M NaCl is moderate, with HA–CHI-71, HA–CHI-88, and HA–CHI-98 having a tan δ (at 0.1 rad s^{-1}) of 0.8, 0.6, and 0.4, respectively. We will come back to this point later.

For all HA–CHI series, the horizontal shift factor, a_s, decreases exponentially with the salt concentration, $a_s \propto \exp(A–B\cdot[NaCl])$ with A and B constants. In the case of HA–CHI-98, a_s does not evolve below 0.2 M NaCl due to kinetic trapping. This exponential salt dependence does not follow the stretched exponential prediction $a_s \propto \exp(A–B\cdot[NaCl]^{1/2})$ based on the sticky Rouse model proposed by Spruijt and colleagues;[13] however, it is in agreement with the other experimental results of several authors.[30,39,41,63,64] In particular, Sun and colleagues[39] found a slope of −10 for HA–CHI complex coacervates based on a CHI with DD in the range of 75 to 85%. While the origin of this discrepancy with the theoretical prediction is unknown,[2] the overall trend, *i.e.*, the acceleration of the dynamics as the salt lowers the activation energy of the macroion pair dissociation, remains consistent with salt acceleration of dynamics in complex coacervates.

An initially surprising result was that the exponential decay of a_s with the salt concentration is dependent on CHI's CD. As seen from the slope of the linear fits on the semi-log plot (Fig. 5A), increasing the CD decreases the sensitivity of the dynamics to salt. This trend is in contrast with the findings of Ramírez Marrero *et al.*[26] and van Westerveld *et al.*,[24,25] who found that the slope of log(a_s) *versus* salt concentration was insensitive to the chemistry and hydrophilicity/hydrophobicity of the comonomers used to adjust the CD. The insensitivity to the CD was arguably attributed to the unchanged identity and strength of the macroion associations in each study.[26] In other words, the only effect of the CD was the dilution of the electrostatic stickers without impacting the relaxation

mechanism. However, these studies used synthetic polyelectrolytes of low molecular weights, where the unentangled dynamics were controlled by macroion-type stickers. These polymers are essentially different from our HA and CHI, both in molecular weight and in chain stiffness. Unlike flexible polyelectrolytes that are ubiquitous in the literature on complex coacervates, both HA and CHI are semi-flexible polyelectrolytes, with persistence lengths that can be 10 to 50 times larger than that of flexible polyelectrolytes, as a function of comonomer composition, CD, salt concentration, and level of hydration.[29,34,65] Such significant changes in the polymer chain stiffness have important consequences for the complex coacervation of the polymers involved.

The salt-sensitivity of the macroion pairing activation energy to the CD in our HA–CHI system is thus a remarkable feature observed with these polysaccharides. We believe that this peculiar dynamic behavior is due to additional contributions to the dynamics by topological constraints (*i.e.* entanglements), kinetic trapping, and hydration. These correlated contributions are closely linked to how the CD of CHI modifies its inherent chain rigidity and complexation with HA.[27,66] Increasing CHI's CD has two main consequences: (i) it increases CHI's persistence length,[36] and (ii) it promotes its complexation and kinetic trapping with HA.[27] With increased l_p, the entanglement density decreases and kinetic trapping becomes more likely. On the other hand, the increased complexation at higher CD increases the polymer content (see Fig. 2), which favors more entanglements, but it can also further stiffen CHI and HA chains as they lose further translational entropy upon complexation. The dynamics of HA–CHI complex coacervates, becoming less salt-sensitive with CHI's CD, suggest that the complexation and kinetic trapping dominate over the increased persistence length of CHI. Once again, these effects are highly correlated, and more systematic investigations are needed to pin down the contribution of each effect, but they clearly do not disturb the time–salt superposition within each series (Fig. 4). We must also emphasize that the variability of the macroion pairing activation energy (Fig. 5A) cannot be due to other weak molecular interactions, which are negligible under the experimental conditions of this study, as mentioned earlier.

In addition to a_s, a small vertical shift factor, b_s, was also used in performing TSS. As shown in Fig. 5B, b_s shows a slight increase with the added salt concentration for all HA–CHI series, but remains on the order of unity. The increase in b_s corresponds to a decrease in the polymer content of the complex coacervates (Fig. S12 in the SI), consistent with the intuition that the vertical shift factor must decrease with the number density of network strands (or the modulus). Although the origin of this salt-dependence remains an open question, the trend observed in our data aligns reasonably with this intuition and with several previous reports[12,15,30] on soft solid-like polyelectrolyte complex coacervates. In any case, the magnitude of this change is considerably smaller than a_s, indicating that the main effect of salt is on the dynamics.

In the case of the samples based on butyryl chitosan (HA–*but*-CHI-88), the values of a_s, are slightly but consistently higher than those of HA–CHI-88, while b_s shows the opposite trend. This indicates that the HA–*but*-CHI-88 system is slightly less dynamic and stiffer, which is also seen from the master curves shown in Fig. 4 or Fig. S11 in the SI. Nevertheless, linear fits to $\log(a_s)$ *versus* salt concentration have similar slopes for HA–CHI-88 and HA–*but*-CHI-88, suggesting that modifying the acetamide residue of CHI to butyryl (*but*-CHI) does not alter the strength (or activation energy) of the macroion associations. The slight modification of the dynamics may be due to a different distribution of small ions and water molecules around the macroion pairs.[26] Understanding the higher plateau modulus (15 kPa for HA–*but*-CHI-88 *vs.* 8 kPa for HA–CHI-88 at 10 rad s^{-1}) is less obvious, as it cannot be solely due to the contribution of the polymer content, which is only slightly higher (0.68 M *vs.* 0.65 M on a monomer basis). This might be linked to the subtle changes in CHI's persistence length, which could modify the length of network strands. A systematic study on the effect of the side chain length is a perspective to verify these hypotheses.

3.3 Time–salt–charge density superposition

Despite different salt sensitivities of the time–salt superposition horizontal shift factors for different HA–CHI series (Fig. 5A), the master curves in Fig. 4 give the impression that the dynamic behavior of the different HA–CHI systems is self-similar. The self-similarity was indeed confirmed *via* van Gurp-Palmen and Cole–Cole analyses (Fig. S14 in the SI). Taking the TSS curve of HA–CHI-88 at 0.4 M NaCl as the reference, we rescaled the dynamics of all the systems onto a universal master curve using a time–salt–charge density superposition (TSCDS). The master curve of HA–*but*-CHI-88 was also successfully rescaled onto the universal master curve, but with all evidence against hydrophobic effects, this was not called a time–salt-hydrophobicity superposition. The universal master curve obtained from the four HA–CHI series is shown in Fig. 6A, with the corresponding $\tan(\delta)$ curves presented in Fig. S13 in the SI. The universal master curve reveals a broad rubbery plateau extending over six decades in frequency and a long reptation time of 210 s.

The horizontal and vertical shift factors a_{CD} and b_{CD}, as a function of CHI's CD are presented in Fig. 6B. The increase in a_{CD} reflects the deceleration of the dynamics (*i.e.* longer relaxation times) with the CD, confirming again that CHI's neutral comonomer is relatively hydrophilic.[24,26] In the case of the HA–*but*-CHI-88, a small increase of a_{CD} suggests that, at least at this CD, changing CHI's acetyl moieties to butyryl has a weak decelerating effect on the dynamics. However, a better understanding of such chemical modifications requires more systematic studies combining the side chain length and the degree of substitution. In the case of b_{CD}, changes remain within the same order of magnitude. A decrease in b_{CD} with CHI's CD corresponds to the higher plateau modulus of the series at higher charge densities. Likewise, the b_{CD} of HA–*but*-CHI-88 is slightly lower compared to HA–CHI-88.

Fig. 7A and B plot the dependence of the universal horizontal shift factor, a_s a_{CD}, on the added salt concentration and on

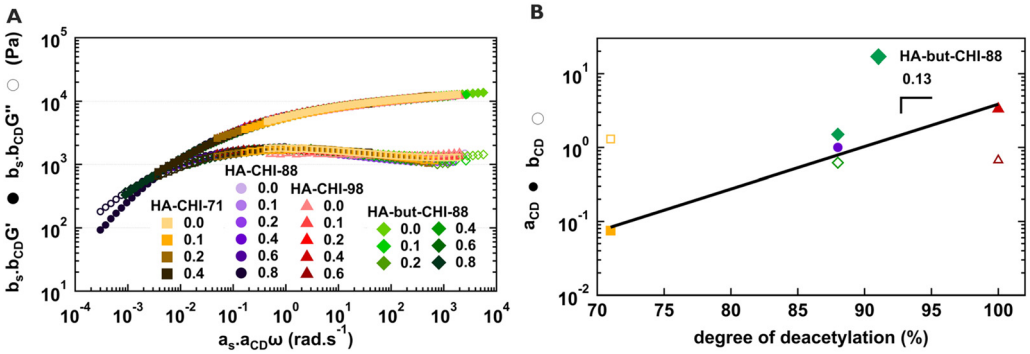

Fig. 6 (A) Rescaled dynamic moduli of HA–CHI-71, HA–CHI-88, HA–CHI-98 and HA–*but*-CHI-88 complex coacervates using time–salt–charge density superposition (TSCDS), taking the HA–CHI-88 TSS master curve at 0.4 M NaCl as the reference. (B) Horizontal and vertical shift factors, a_{CD} and b_{CD}, as a function of CHI's degree of deacetylation.

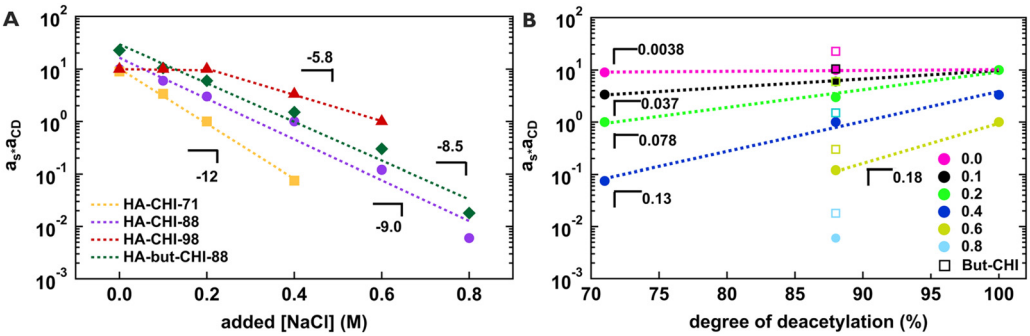

Fig. 7 Universal horizontal shift factor, $a_s\,a_{CD}$ as a function of (A) added salt concentration and (B) CHI's degree of deacetylation, with the HA–CHI-88 TSS master curve at 0.4 M NaCl as the reference.

CHI's CD, respectively. Variations in $a_s\,a_{CD}$ with the salt concentration follow the same exponential behavior as that observed with a_s (*i.e.* they have the same slopes on a semi-log plot), but with a vertical shift a_{CD} accounting for the change in CHI's CD (and the chemical modification of CHI's acetyl function to butyryl in the case of HA–*but*-CHI-88). As discussed in the section on TSS (see Fig. 5A), higher charge densities lower the sensitivity of HA–CHI dynamics to the added salt concentration. We proposed that this is due to the convoluted effects of the increased CD and the persistence length of CHI.

Fig. 7B corroborates these interpretations from another perspective. In this case, $a_s\,a_{CD}$ is shown as a function of CHI's CD, with each color marking samples prepared at a given salt concentration. As the added salt concentration is increased, a growing exponential dependence of the universal horizontal shift factor on CHI's CD is observed, suggesting that these complex coacervates are in the charge-dominated regime.[22,24,26] This is also consistent with their phase behavior (see Fig. 2). In the case of no added salt (0.0 M NaCl), the horizontal shift factor, and thus the relaxation dynamics, is almost independent of the CD. This once again indicates that the dynamics at no added salt are dominated by a combination of topological and kinetic trapping rather than by purely dynamic macroion associations. At higher salt concentrations, kinetic trapping is increasingly attenuated, as the number and strength of macroion associations decrease, making them more dynamic. Higher salt concentrations also reduce the l_p of both polymers. While this tends to increase the entanglement density at a given polymer concentration, the significant decrease in the polymer content upon swelling (see Fig. 2) effectively reduces the entanglement density, as witnessed by the salt-induced decrease in the plateau modulus (Fig. 3 and Fig. S7 in the SI). Together, these effects increase the importance of the CD in determining the complex coacervate dynamics at higher salt concentrations. The fact that the exponential growth of the universal shift factor with the CD is not unique to all salt concentrations is a new finding with HA–CHI complex coacervates. We believe that this has to do with the high molecular weight of these polymers and, especially, with their inherent chain rigidity. Thus, a similar viscoelastic behavior is expected with other semi-flexible polyelectrolytes, a topic that merits further investigation.

An interesting point in Fig. 7 is that we can find complex coacervates with identical relaxation dynamics, although they are obtained at different salt concentrations and with CHI of different DD. This is, for instance, the case for HA–CHI-71 at 0.2 M NaCl, HA–CHI-88 at 0.4 M NaCl, and HA–CHI-98 at 0.6 M NaCl. These samples are also very close in terms of the plateau modulus, given that the universal vertical shift factor is close to unity. The equivalence of the viscoelastic properties across different combinations of CD and salt concentration highlights a new degree of tunability in these bio-sourced materials.

Consequently, one can design materials with targeted viscoelastic properties not only by controlling the salt concentration but also by adjusting the CD. This allows for the customization of material performance, particularly in biomedical applications where the salt concentration is fixed (physiological, *i.e.*, 0.15 M NaCl).

To the best of our knowledge, this is the first report of a TSCDS for highly entangled complex coacervates, with all previous reports focusing on unentangled systems based on model polyelectrolytes.[22,24,26] This also marks the first TSCDS for a biosourced system based on semi-flexible polyelectrolytes. Even in highly entangled systems, enabled by the high molecular weight of the polymers used,[42] changes in salt concentration, CD, or replacement of the neutral comonomer's acetyl moiety with a less polar group do not alter the relaxation mechanism of the material, but only the time scale over which relaxation occurs. A key difference from unentangled systems is the necessity of applying a vertical shift factor to achieve a successful superposition. This reflects that, in the entangled network, the contribution of macroion-type stickers to the shear modulus is negligible compared to that of the entanglements.

3.4 Underwater adhesion

We next studied the underwater adhesiveness of all HA–CHI complex coacervates in pull-off experiments performed in the supernatant at 37 °C at a nominal strain rate of 0.2 s^{-1}. The nominal stress–strain curves presented in Fig. S16 in the SI show certain differences among the HA–CHI series as a function of CHI's DD and within each series as a function of the added salt. The samples at 0.0 to 0.2 M NaCl are generically characterized by a peak stress at small strains below 10% followed by a sharp drop and adhesive detachment at strains below 100%. The samples at 0.4 M NaCl and higher salt concentrations were uninteresting materials as adhesives, featuring smaller peaks in adhesion stress and liquid-like failure. We will discuss these differences in terms of the adhesion strength, σ_{max}, and the work of adhesion, W_{adh}. These parameters are shown in Fig. 8A and B, respectively.

For the series with different charge densities, the adhesion strength increases with NaCl concentration from 0.0 to 0.2 M, above which it decreases rapidly due to the salt-induced softening of the complexes. The work of adhesion of HA–CHI-88 and HA–CHI-98 follows a similar trend, reaching 7 J m^{-2} at 0.2 M NaCl, followed by a significant decrease toward the salt resistance of each complex. However, in the case of HA–CHI-71, W_{adh} monotonously decreases from 8 J m^{-2} at 0.0 M NaCl. Apart from these general trends, comparisons across the different series do not suggest a conclusive trend as a function of chitosan's DD. This is particularly evident in σ_{max}. For example, HA–CHI-71, HA–CHI-88, and HA–CHI-98 at 0.2 M have an adhesion strength of 74, 43, and 57 kPa, respectively. Nevertheless, the acetyl series have an optimal performance at 0.2 M NaCl, which seems to coincide with the disappearance of the kinetic trapping and the slight softening of the materials (see Fig. 8).

The frequency sweeps of the HA–CHI complex coacervates (Fig. 3A, B and Fig. S7 in the SI) show that, while these materials are all soft enough to meet the Dahlquist criterion ($G' < 10^5$ Pa at 1 Hz), most of them lack a sufficiently dissipative nature ($\tan\delta < 0.3$) to perform as underwater pressure-sensitive adhesives (PSA). Indeed, the TSCDS master curve (Fig. 6A) reveals the highly elastic and non-dissipative nature of these materials on the time scale of the adhesion experiments. Unlike PSA, which are in the upper half of the rubbery plateau and the transition region, *i.e.*, in the vicinity of the segmental relaxation time, HA–CHI complex coacervates have significantly shorter relaxation times due to their large water content. The indifference to compositional changes with the CD (see Fig. 2) may be understood as the failure of these materials to form an intimate contact with the probe, resulting in early adhesive detachment regardless of the composition.

Overall, the underwater adhesive performance of these materials is comparable to that of medium- to high-molecular-weight HA–CHI complex coacervates under wet[42] and immersed[30] conditions. The higher *wet* adhesion strengths, reported by Parisi's group,[42] are probably mostly due to the larger confinement level (r/h_0, where r is the probe radius and h_0 is the adhesive thickness) of the adhesive layer and not necessarily the absence of an aqueous medium. As correctly pointed out by the same authors, the adhesive properties of these materials are mainly controlled by the entangled mesh of semi-rigid HA and CHI. *Via* a systematic variation of low, medium, and high molecular weight combinations of HA

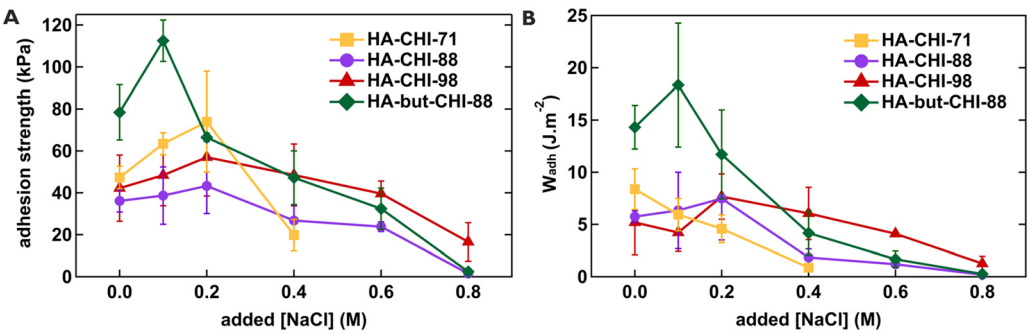

Fig. 8 Underwater adhesion results for HA–CHI complex coacervates immersed in their supernatant at 37 °C: (A) adhesion strength and (B) work of adhesion as a function of the added salt concentration.

and CHI, they concluded that HA, with its inherently higher stiffness and strong hydration, dominates the mechanical response of these complex coacervates. The moderate effect of CHI's CD on the adhesive properties of our complex coacervates, all of which are based on the same HA, is aligned with this interpretation.

Interestingly, HA–*but*-CHI-88 appears relatively stronger, more deformable, and more dissipative (see Fig. 8 and Fig. S16 in the SI) than all the other HA–CHI systems from 0.0 M to 0.1 M NaCl. At 0.1 M NaCl, this material is characterized by a σ_{max} of 110 kPa and a W_{adh} of 18 J m^{-2}, placing it among the most performant coacervate-based (underwater) adhesives without an external trigger.[24,25,30,41,42,67–72] The performance of this water-rich adhesive is also among the highest values reported for systems based on other weak molecular interactions.[25,68–71,73–75] At 0.2 M NaCl, HA–*but*-CHI-88 has a comparable adhesion strength to the other samples, but it is more deformable, resulting in a W_{adh} of 12 J m^{-2}. With the typical softening of the complex coacervate at higher salt concentrations, the adhesive properties gradually decrease in a similar manner to the other complex coacervates.

It might be argued that the higher adhesion strength of HA–*but*-CHI-88 compared to HA–CHI-88 at low salt concentrations is proportionate to their respective storage modulus. However, this argument is not valid for HA–CHI-98, which has the same G' as HA–*but*-CHI-88 but a much lower adhesion strength (48 kPa). Moreover, these three samples have tan δ below 0.3. While linear viscoelastic criteria are helpful in designing underwater adhesives, they are not sufficient for explaining all the complexities of adhesion, especially under immersed conditions.[9,76] We believe that the distinct adhesion performance of HA–*but*-CHI-88 at 0.1 M NaCl is not due to the subtle differences in linear viscoelasticity, but rather due to the chemical modification of CHI with apolar butyryl moieties, which enable a better removal or restructuration of interfacial water in favor of better contact formation. A 10 mol% degree of substitution may appear too small to cause such differences in the adhesive behavior. However, the polarity of classic PSA is typically modified with minimal variations of 2 to 10 mol% in comonomer composition to enhance the performance of the formulation on high or low energy substrates.[77–79] Such differences in surface energy are not observable by linear rheological measurements. Not to mention, once again, that the rheological behavior of these complex coacervates is dominated by the larger and stiffer HA, rather than CHI.

Among the complex coacervates developed in this work, HA–*but*-CHI-88 at 0.1 M NaCl was identified as the most promising candidate for an underwater adhesive. This formulation combines good underwater performance with aqueous stability at near-physiological salinity.[72,80] While these HA–CHI complexes do not have the characteristic behavior of highly deformable and dissipative PSA, they can be designed to have high adhesion strengths, as shown in the present work. Moreover, previous reports by our team[30] and others[81] have shown the potential of HA–CHI complex coacervates for biomedical applications. One aspect that merits investigation in future work is how the chemical modification of CHI may change certain biological activities of this polymer and its complexes with other polymers. Beyond these biological considerations, future efforts to enhance adhesion properties must focus on strategies to obtain complex coacervates with reduced water content and, conversely, higher polymer fractions. In this context, the use of crowding agents may prove beneficial. Additionally, tuning the system to achieve segmental relaxation times comparable to those of conventional PSA will be of great interest.

4. Summary and conclusions

In this study, we investigated the effect of charge density (CD) on the phase behavior, viscoelasticity, and underwater adhesion of complex coacervates formed from high-molecular-weight, semi-flexible polyelectrolytes. For this, we varied the DD of chitosan (from 71 to 98%) at constant molecular weight in combination with hyaluronic acid. Increasing CHI's CD increased the number of macroion pairs (*i.e.* stickers) per chain, which affected the complex coacervate composition, expanding the two-phase region of the state diagram and favoring kinetic trapping. We further studied the linear viscoelastic properties of HA–CHI complex coacervates. The majority of the complex coacervates were soft viscoelastic solids within the lower frequency end of the rubbery plateau. Increasing the added salt concentration moderately decreased the plateau modulus but significantly reduced the reptation relaxation time. Time–salt superposition (TSS) was successfully applied to each HA–CHI system, indicating that macroion pairs dominate the salt-dependent relaxation dynamics. The individual TSS master curves (for HA–CHI series at different CD) were successfully rescaled onto a universal master curve using a time–salt–charge density superposition (TSCDS). The deceleration of the dynamics (*i.e.*, longer relaxation times) with increasing CD confirmed the relatively hydrophilic character of CHI's neutral comonomer and indicated that the systems were in the charge-dominated regime. We found that the salt sensitivity of these HA–CHI complex coacervates depended on CHI's charge density, and *vice versa*. This peculiar behavior not observed with flexible, unentangled polyelectrolytes, is due to varying degrees of kinetic trapping and entanglements among these HMW, semi-flexible polymers. A key difference from unentangled systems is the application of a small vertical shift factor (on the order of unity) for a successful superposition. Based on these results, we proposed that the contribution of macroion-type stickers to the shear modulus of entangled network is negligible compared to that of the entanglements.

We then investigated the relationship between the viscoelasticity and the adhesion properties of different HA–CHI complex coacervates. While these materials were sufficiently soft to meet the Dahlquist criterion (plateau modulus below 0.1 MPa at 1 Hz), they were not sufficiently dissipative. Nevertheless, they exhibited adhesion strengths of up to 74 kPa when immersed in their own supernatant. All HA–CHI series showed optimal performance at 0.2 M NaCl, which appears to coincide

with the disappearance of kinetic trapping and a slight softening of the materials. No conclusive trend was observed as a function of chitosan's CD, likely due to the use of the same HA in all systems. Indeed, it is likely that the adhesive properties are governed by the semi-flexible mesh of entangled HA and CHI.

We also explored complex coacervates of HA with a chemically modified CHI (DD = 88%), where the acetyl moiety of the neutral comonomer was replaced with a less polar butyryl moiety (called HA–*but*-CHI-88). Comparing it to HA–CHI-88, no significant differences in the phase composition were observed, suggesting that the glucosamine comonomer of CHI is sufficiently hydrophilic at the comonomer fractions (10%) and acyl chain length used in this work. Regarding viscoelastic properties, a slightly less dynamic and stiffer system was observed, without altering the strength of the macroion associations. Interestingly, HA–*but*-CHI-88 at 0.1 M NaCl emerged as the most promising underwater adhesive among the complex coacervates studied here. This formulation appeared stronger, more deformable, and more dissipative than the other HA–CHI systems, exhibiting an adhesion strength of 110 kPa and an adhesion energy of 18 J m^{-2}. It was proposed that the superior performance of this coacervate is due to the higher efficiency of the apolar butyryl moieties at removing interfacial bound water to facilitate better contact with the substrate. This bio-sourced coacervate is among the most high-performing coacervate-based underwater adhesives at near-physiological salt concentrations.

This study highlights the importance of the charge density and inherent chain rigidity of polyelectrolytes in controlling the composition and mechanical behavior of entangled complex coacervates. The findings of this study will be useful in understanding other systems based on semi-flexible polymers, opening new perspectives for the design of complex coacervates, for example by modifying the charge density and/or the comonomer chemistry. Moving forward, it will be of great interest to characterize the nanostructure of these complex coacervates. In particular, it will be interesting to quantify changes in the persistence length of the polymers involved at different charge densities and salt concentrations.

Author contributions

Maxime Precheur: data curation, methodology, validation, formal analysis, investigation, visualization, and writing – original draft; Ali Kanan: data curation, formal analysis, and investigation; Alexei Dmitrievitsj Filippov: validation, formal analysis, visualization, and writing – review & editing; Kylian Virieux: resources and data curation; Stéphane Trombotto: formal analysis, visualization, and writing – review & editing; Fouzia Boulmedais: conceptualization, project administration, supervision, validation, visualization, and writing – review & editing. Mehdi Vahdati: conceptualization, funding acquisition, project administration, supervision, validation, visualization, and writing – review & editing.

Conflicts of interest

There are no conflicts to declare.

Data availability

All raw and processed data of this study are available from the corresponding author upon reasonable request. The data is not currently deposited in a public repository due to specific file types from different instruments, which require instrument-specific software to access. Upon request, the raw files, exported CSV files, and Igor Pro® analysis files will be made available *via* a secure link or institutional database.

Supplementary information (SI): details of chemical modification methods, characterization of polymers by SEC, compositional analysis by TGA and the related calculations, calculations of the doping level, individual phase diagrams in molarity and mass fractions, linear viscoelastic analyses (additional frequency sweeps, Cole–Cole and van Gurp Palmen plots, and shift factors), and underwater adhesion (stress–strain curves). See DOI: https://doi.org/10.1039/d5sm01220a.

Acknowledgements

The authors would like to thank Leandro Jacomine and Wiebke Drenckhan (CNRS, Institut Charles Sadron) for access to the rheometer of the INCA platform of ICS. The authors also thank CARMAC and Matte'Rheo platforms of ICS. MV acknowledges Agence Nationale de la Recherche (ANR-22-CPJ2-0122-01) and the Région Grand-Est (convention no. 23E00092713) for financial support. This work of the Interdisciplinary Institute HiFunMat, as part of the ITI 2021-2028 program of the University of Strasbourg, CNRS and Inserm, was supported by IdEx Unistra (ANR-10-IDEX-0002) and SFRI (STRAT'US project, ANR-20-SFRI-0012) under the framework of the French Investments for the Future Program.

References

1 C. E. Sing and S. L. Perry, *Soft Matter*, 2020, **16**, 2885–2914.
2 S. M. Lalwani, C. I. Eneh and J. L. Lutkenhaus, *Phys. Chem. Chem. Phys.*, 2020, **22**, 24157–24177.
3 Q. Wang and J. B. Schlenoff, *Macromolecules*, 2014, **47**, 3108–3116.
4 J. Zheng, P. Van der Meeren and W. Sun, *Aggregate*, 2023, **5**, e449.
5 C. E. Sing, *Adv. Colloid Interface Sci.*, 2017, **239**, 2–16.
6 S. Chen and Z.-G. Wang, *Proc. Natl. Acad. Sci. U. S. A.*, 2022, **119**, e2209975119.
7 Q. Peng, T. Wang, D. Yang, X. Peng, H. Zhang and H. Zeng, *Prog. Polym. Sci.*, 2024, **153**, 101827.
8 J. P. Jones, M. Sima, R. G. O'Hara and R. J. Stewart, *Adv. Healthcare Mater.*, 2016, **5**, 795–801.
9 M. Vahdati, D. Hourdet and C. Creton, *Prog. Polym. Sci.*, 2023, **139**, 101649.

10 A. N. Kwant, J. S. Es Sayed, M. Kamperman, J. K. Burgess, D. J. Slebos and S. D. Pouwels, *Adv. Healthcare Mater.*, 2025, **14**, 2402340.
11 K. Akkaoui, M. Yang, Z. A. Digby and J. B. Schlenoff, *Macromolecules*, 2020, **53**, 4234–4246.
12 F. G. Hamad, Q. Chen and R. H. Colby, *Macromolecules*, 2018, **51**, 5547–5555.
13 E. Spruijt, J. Sprakel, M. Lemmers, M. A. C. Stuart and J. Van Der Gucht, *Phys. Rev. Lett.*, 2010, **105**, 208301.
14 A. B. Marciel, S. Srivastava and M. V. Tirrell, *Soft Matter*, 2018, **14**, 2454–2464.
15 Y. Liu, B. Momani, H. H. Winter and S. L. Perry, *Soft Matter*, 2017, **13**, 7332–7340.
16 J. R. Vieregg, M. Lueckheide, A. B. Marciel, L. Leon, A. J. Bologna, J. R. Rivera and M. V. Tirrell, *J. Am. Chem. Soc.*, 2018, **140**, 1632–1638.
17 S. L. Perry, L. Leon, K. Q. Hoffmann, M. J. Kade, D. Priftis, K. A. Black, D. Wong, R. A. Klein, C. F. Pierce, K. O. Margossian, J. K. Whitmer, J. Qin, J. J. De Pablo and M. Tirrell, *Nat. Commun.*, 2015, **6**, 6052.
18 S. Tabandeh and L. Leon, *Molecules*, 2019, **24**, 868.
19 S. L. Perry, Y. Li, D. Priftis, L. Leon and M. Tirrell, *Polymers*, 2014, **6**, 1756–1772.
20 L. Li, A. M. Rumyantsev, S. Srivastava, S. Meng, J. J. De Pablo and M. V. Tirrell, *Macromolecules*, 2021, **54**, 105–114.
21 S. Ali and V. M. Prabhu, *Gels*, 2018, **4**, 11.
22 J. Huang, F. J. Morin and J. E. Laaser, *Macromolecules*, 2019, **52**, 4957–4967.
23 A. E. Neitzel, Y. N. Fang, B. Yu, A. M. Rumyantsev, J. J. De Pablo and M. V. Tirrell, *Macromolecules*, 2021, **54**, 6878–6890.
24 L. van Westerveld, T. Pelras, A. H. Hofman, K. Loos, M. Kamperman and J. Es Sayed, *Macromolecules*, 2024, **57**, 652–663.
25 L. van Westerveld, J. Es Sayed, M. de Graaf, A. H. Hofman, M. Kamperman and D. Parisi, *Soft Matter*, 2023, **19**, 8832–8848.
26 I. A. Ramírez Marrero, L. Boudreau, W. Hu, R. Gutzler, N. Kaiser, B. von Vacano, R. Konradi and S. L. Perry, *Macromolecules*, 2024, **57**, 4680–4694.
27 C. F. Narambuena, E. P. M. Leiva, M. Chávez-Páez and E. Pérez, *Polymer*, 2010, **51**, 3293–3302.
28 E. Buhler and F. Boué, *Macromolecules*, 2004, **37**, 1600–1610.
29 S. Morariu, C.-E. Brunchi and M. Bercea, *Ind. Eng. Chem. Res.*, 2012, **51**, 12959–12966.
30 P. Galland, M. H. Iqbal, D. Favier, M. Legros, P. Schaaf, F. Boulmedais and M. Vahdati, *J. Colloid Interface Sci.*, 2024, **661**, 196–206.
31 Y. Kang, X. Zhao, X. Han, X. Ji, Q. Chen, H. Pasch, A. Lederer and Y. Liu, *Carbohydr. Polym.*, 2021, **271**, 118402.
32 M. Rinaudo, *Prog. Polym. Sci.*, 2006, **31**, 603–632.
33 F. Alsaikhan and B. Farhood, *Int. J. Biol. Macromol.*, 2024, **280**, 135893.
34 J. P. Berezney and O. A. Saleh, *Macromolecules*, 2017, **50**, 1085–1089.
35 F. Horkay, P. J. Basser, D. J. Londono, A. M. Hecht and E. Geissler, *J. Chem. Phys.*, 2009, **131**, 184902.
36 Y. Kang, X. Zhao, X. Han, X. Ji, Q. Chen, H. Pasch, A. Lederer and Y. Liu, *Carbohydr. Polym.*, 2021, **271**, 118402.
37 M. Rinaudo, *Prog. Polym. Sci.*, 2006, **31**, 603–632.
38 J. Es Sayed, C. Caïto, A. Arunachalam, A. Amirsadeghi, L. van Westerveld, D. Maret, R. A. Mohamed Yunus, E. Calicchia, O. Dittberner, G. Portale, D. Parisi and M. Kamperman, *Macromolecules*, 2023, **56**, 5891–5904.
39 J. Sun, J. D. Schiffman and S. L. Perry, *ACS Appl. Polym. Mater.*, 2022, **4**, 1617–1625.
40 M. Balima, I. Morfin, G. Sudre and A. Montembault, *Carbohydr. Polym.*, 2024, 122265.
41 M. Vahdati, F. J. Cedano-Serrano, C. Creton and D. Hourdet, *ACS Appl. Polym. Mater.*, 2020, **2**, 3397–3410.
42 R. A. Mohamed Yunus, R. Poelman, A. Arunachalam, M. Kamperman and D. Parisi, *Soft Matter*, 2025, **21**, 8935–8950.
43 C. Garreau, L. Chiappisi, S. Micciulla, N. Blanc, I. Morfin, A. Desorme, T. Mignot, S. Trombotto, T. Delair and G. Sudre, *Int. J. Biol. Macromol.*, 2023, **245**, 125565.
44 A. B. Kayitmazer, F. Comert, H. H. Winter and P. B. Messersmith, *Biomolecules*, 2022, **12**, 1817.
45 L. Li, S. Srivastava, M. Andreev, A. B. Marciel, J. J. De Pablo and M. V. Tirrell, *ACS Macro Lett.*, 2018, **51**, 2988–2995.
46 L. W. Chang, T. K. Lytle, M. Radhakrishna, J. J. Madinya, J. Vélez, C. E. Sing and S. L. Perry, *Nat. Commun.*, 2017, **8**, 1273.
47 Y. Liu, H. H. Winter and S. L. Perry, *Adv. Colloid Interface Sci.*, 2017, **239**, 46–60.
48 K. Akkaoui, Z. A. Digby, C. Do and J. B. Schlenoff, *Macromolecules*, 2024, **57**, 1169–1181.
49 J. T. G. Overbeek and M. J. Voorn, *J. Cell. Comp. Physiol.*, 1957, **49**, 7.
50 E. Spruijt, A. H. Westphal, J. W. Borst, M. A. Cohen Stuart and J. Van Der Gucht, *Macromolecules*, 2010, **43**, 6476–6484.
51 A. Reisch, P. Tirado, E. Roger, F. Boulmedais, D. Collin, J. C. Voegel, B. Frisch, P. Schaaf and J. B. Schlenoff, *Adv. Funct. Mater.*, 2013, **23**, 673–682.
52 R. F. Shamoun, A. Reisch and J. B. Schlenoff, *Adv. Funct. Mater.*, 2012, **22**, 1923–1931.
53 S. Meng, J. M. Ting, H. Wu and M. V. Tirrell, *Macromolecules*, 2020, **53**, 7944–7953.
54 Z. A. Digby, M. Yang, S. Lteif and J. B. Schlenoff, *Macromolecules*, 2022, **55**, 978–988.
55 J. B. Schlenoff, M. Yang, Z. A. Digby and Q. Wang, *Macromolecules*, 2019, **52**, 9149–9159.
56 V. M. S. Syed and S. Srivastava, *ACS Macro Lett.*, 2020, **9**, 1067–1073.
57 Y. Liu, C. F. Santa Chalarca, R. N. Carmean, R. A. Olson, J. Madinya, B. S. Sumerlin, C. E. Sing, T. Emrick and S. L. Perry, *Macromolecules*, 2020, **53**, 7851–7864.
58 E. Spruijt, M. A. Cohen Stuart and J. Van Der Gucht, *Macromolecules*, 2013, **46**, 1633–1641.
59 M. Rubinstein and R. H. Colby, *Polymer Physics*, Oxford University Press, 2003.
60 E. Santiago De Alvarenga, *Biotechnol. Biopolym.*, 2011, **24**, 91–108.

61 Q. Z. Wang, X. G. Chen, N. Liu, S. X. Wang, C. S. Liu, X. H. Meng and C. G. Liu, *Carbohydr. Polym.*, 2006, **65**, 194–201.
62 P. Sorlier, A. Denuziè, C. Viton and A. Domard, *Biomacromolecules*, 2001, **2**, 765–772.
63 A. B. Marciel, S. Srivastava and M. V. Tirrell, *Soft Matter*, 2018, **14**, 2454–2464.
64 K. Sadman, Q. Wang, Y. Chen, B. Keshavarz, Z. Jiang and K. R. Shull, *Macromolecules*, 2017, **50**, 9417–9426.
65 S. J. de, M. Alves, M. A. Santos, J. E. da, S. Neto, H. N. da Silva, M. C. S. Barbosa, M. V. L. Fook, R. F. Navarro and S. M. de L. Silva, *Gels*, 2025, **11**, 212.
66 M. O. Khan and D. Y. C. Chan, *Macromolecules*, 2005, **38**, 3017–3025.
67 H. H. Winter and M. Mours, *Adv. Polym. Sci.*, 1997, **134**, 165–234.
68 M. Dompé, F. J. Cedano-Serrano, O. Heckert, N. van den Heuvel, J. van der Gucht, Y. Tran, D. Hourdet, C. Creton and M. Kamperman, *Adv. Mater.*, 2019, **31**, 1808179.
69 M. Dompé, F. J. Cedano-Serrano, M. Vahdati, L. van Westerveld, D. Hourdet, C. Creton, J. van der Gucht, T. Kodger and M. Kamperman, *Adv. Mater. Interfaces*, 2020, **7**, 1901785.
70 D. Lee, H. Hwang, J. S. Kim, J. Park, D. Youn, D. Kim, J. Hahn, M. Seo and H. Lee, *ACS Appl. Mater. Interfaces*, 2020, **12**, 20933–20941.
71 Y. J. Wang, Y. He, S. Y. Zheng, Z. Xu, J. Li, Y. Zhao, L. Chen and W. Liu, *Adv. Funct. Mater.*, 2021, **31**, 2104296.
72 M. Dompé, F. J. Cedano-Serrano, O. Heckert, N. van den Heuvel, J. van der Gucht, Y. Tran, D. Hourdet, C. Creton and M. Kamperman, *Adv. Mater.*, 2019, **31**, 1808179.
73 L. Barbier, P. Pipart, M. Vahdati, C. Lorthioir, Y. Tran and D. Hourdet, *Carbohydr. Polym.*, 2024, **336**, 122126.
74 I. A. van Hees, A. H. Hofman, M. Dompé, J. van der Gucht and M. Kamperman, *Eur. Polym. J.*, 2020, **141**, 110034.
75 M. Vahdati, G. Ducouret, C. Creton and D. Hourdet, *Macromol. Rapid Commun.*, 2020, **41**, 1900653.
76 C. Creton, G. Hu, F. Deplace, L. Morgret and K. R. Shull, *Macromolecules*, 2009, **42**, 7605–7615.
77 A. Lindner, T. Maevis, R. Brummer, B. Lühmann and C. Creton, *Langmuir*, 2004, **20**, 9156–9169.
78 H. Lakrout, P. Sergot and C. Creton, *J. Adhes.*, 1999, **69**, 307–359.
79 H. Lakrout, C. Creton, D. Ahn and K. R. Shull, *Macromolecules*, 2001, **34**, 7448–7458.
80 S. L. Turgeon, C. Schmitt and C. Sanchez, *Curr. Opin. Colloid Interface Sci.*, 2007, **12**, 166–178.
81 O. Karabiyik Acar, A. B. Kayitmazer and G. Torun Kose, *Biomacromolecules*, 2018, **19**, 1198–1211.